Peripheral Stator of the Yeast V-ATPase: Stoichiometry and Specificity of Interaction between the EG Complex and Subunits C and H†

James Féthière,*,‡ David Venzke,‡ Dean R. Madden,§ and Bettina Böttcher‡

Structural and Computational Biology Unit, European Molecular Biology Laboratory, Meyerhofstrasse 1, 69117 Heidelberg, Germany, and Biochemistry Department, Dartmouth Medical School, 7200 Vail Building, Hanover, New Hampshire 03755

Received September 1, 2005; Revised Manuscript Received October 4, 2005

ABSTRACT: V-ATPases are multisubunit membrane protein complexes that use the energy provided by ATP hydrolysis to generate a proton gradient across various intracellular and plasma membranes. In doing so, they maintain an acidic pH in the lumen of intracellular organelles and acidify extracellular milieu to support specific cellular functions. V-ATPases are structurally similar to the F_1F_0-ATP synthase, with an intrinsic membrane domain (V_0) and an extrinsic peripheral domain (V_1) joined by several connecting elements. To gain a clear functional understanding of the catalytic mechanism, and of the stability requirements for regulatory processes in the enzyme, a clear topology of the enzyme has to be established. In particular, the composition and arrangement of the peripheral stator subunits must be firmly settled, as these play specific roles in catalysis and regulation. We have designed a strategy allowing us to coexpress different combinations of these subunits to delineate specific interactions. In this study, we report the interaction between the peripheral stator EG complex and subunits C and H of the V-ATPase from the yeast *Saccharomyces cerevisae*. A combination of analytical gel filtration, native gel electrophoresis, and ultracentrifugation analysis allowed us to ascertain the homogeneity and molar mass of the purified EGC complex as well as of the EG complex, supporting the formation of 1:1(:1) stoichiometric complexes. The EGC complex can be formed in vitro by combining equimolar amounts of subunit C and the EG subcomplex and results most likely from the initial interaction between subunits E and C.

Local regulation of cytosolic pH is critical for several intracellular processes (*1*). Numerous pumps and transporters work in concert to support this tight regulation, and among these, the vacuolar ATPase (V-ATPase)[1] has a central role (*2*, *3*). In eukaryotes, it is responsible for maintaining an acidic pH in several intracellular organelles, which is necessary for the diverse functionalities of these organelles (*2*−*4*). In addition, several specialized cells express the V-ATPase at their plasma membranes for secretion of intracellular protons and acidification of the extracellular environment (*5*−*8*). The enzyme is a multisubunit complex that utilizes the energy provided by ATP hydrolysis to pump protons across membranes. It is composed of 13 distinct subunits that are segregated in two functional domains. This two-part morphology observed from electron microscopy analysis is reminiscent of that of the F-type ATPase, with which it shares numerous topological features (*2*, *9*). One domain, V_0, forms a quarter of the total mass of the enzyme and resides in the membrane. It is composed of five distinct subunits that form the core of a rotating molecular motor that pumps protons using the energy provided by ATP hydrolysis. The other domain, V_1, accounts for the remaining mass of the complex and faces the cytoplasm. It harbors the central catalytic machinery consisting of four subunits and a series of peripheral stators formed by four additional subunits. These are responsible for holding the catalytic head immobile with respect to the rotating V_0 domain.

In addition, these peripheral subunits have been shown to play an important role in the regulation of the enzyme by reversible disassembly (*10*−*13*) and, therefore, require a tight regulation of their structural stability to simultaneously account for efficient catalysis and reversible disassembly. Although topological and mechanistic characteristics of V-ATPases are similar to those of the F-ATPases, this metabolic regulation by reversible dissociation of the subdomains is unique to the V-ATPase family. In addition, whereas F-ATPases show a relatively simple stator (*14*−*16*), this region in V-ATPases is sufficiently complex to be considered as a separate subdomain, consistent with its apparent regulatory role. Specific interactions among these peripheral subunits may thus provide the requisite functional flexibility. If so, it will be necessary to have a detailed biochemical and structural understanding of the topological arrangement of the whole V_1 domain to unravel the mechanistic relationship between regulation and activity.

For several years now, many groups have been addressing this question by applying different techniques. Detailed chemical cross-linking, precipitation and yeast two-hybrid assays, isolation of native subcomplexes, and in vitro

† This work was supported in part by the Deutsch Forschungsgemeinschaft (J.F. and B.B.), the 3D-repertoire EU Network of Excellence grant, and Howard Hughes Medical Institute Award 76200-560801 to Dartmouth Medical School (D.R.M.).

* To whom correspondence should be addressed. Telephone: +49-6221-387-265. Fax: +49-6221-387-519. E-mail: fethiere@embl.de.

‡ European Molecular Biology Laboratory.

§ Dartmouth Medical School.

[1] Abbreviations: V-ATPase, vacuolar ATPase; SEC, size exclusion chromatography.

10.1021/bi051762f CCC: $30.25
Published on Web 11/10/2005

reconstitution of V_1 have provided further insights into the assembly pathway of the enzyme and allowed the identification of subunit interactions (*17*−*23*). In addition, the complexity of the V_1 domain with its connecting regions has been supported by electron microscopy analysis that led to tentative propositions for the topology of the enzyme (*24*−*29*). However, given the available resolution, the electron microscopic analysis relies heavily on the unambiguous biochemical dissection of the nature and number of each component present in the complexes being studied.

It is now well established that subunits E and G form part of the stator, and recently, the crystal structure of subunit C has provided evidence of its participation in the stator, together with some insights into the regulatory mechanism (*30*). However, considerable uncertainty still exists regarding the stoichiometry of these subunits and the number of stators present. It has been proposed that as many as three or four E subunits can assemble (*19*, *31*), and an E dimer has also been postulated (*19*). On the other hand, quantitative amino acid analysis of the coated vesicle V-ATPase indicated the presence of only a single copy of subunit E per complex (*32*). Similar analysis suggests that two G subunits are present (*17*), and there are reports as well that the G subunit forms a dimer in solution (*33*). Finally, cross-linking studies have identified the presence of a 1:1 EG complex (*17*). These various types of evidence show that, although we are approaching a sketch of the topological map of the stator, important discrepancies still exist regarding the stoichiometry of interaction of the different subunits.

Reconstitution of defined subcomplexes offers an alternative to the analysis of subcomplexes isolated from native membranes. Active V-ATPase reconstituted from recombinant subunits has been achieved previously and shown to be valuable in providing a tool for studying subunit-dependent activity of the enzyme and subunit interactions (*34*). However, some of the subunits could not be produced in their native conformation and required refolding protocols, which may account for differences observed in the activity of the enzyme. We have adopted a strategy that enables us to systematically investigate subunit interactions step by step, with the ultimate goal of reconstructing an intact active recombinant V_1 domain for functional and structural studies. The coexpression strategy we have developed is a valuable tool for assessing the topology-dependent activity and regulation of the enzyme. In addition, it allows us to systematically produce defined subcomplexes and study their biophysical properties independently. Furthermore, it allows us to avoid the potential stoichiometric bias introduced in in vitro reconstituted complexes. Building on our first investigation of the EG complex (*35*), we now show that this complex can associate with subunit C, forming 1:1 and 1:1:1 stoichiometric complexes. In addition, we report the isolation of an EGH complex using the same strategy.

EXPERIMENTAL PROCEDURES

Cloning and Expression. Subunits C and H were cloned by PCR from a *Saccharomyces cerevisae* genomic DNA library as a template (gift from M. Knopp, European Molecular Biology Laboratory). Primers were CATGCCATGGCTACTGCGTTATATACT (forward-C), CATGTCCATGGGCGCAACCAAAATTTTAATG (forward-H), GGGGTACCTTATAAATTGATTATATACATCACA (reverse-C), and CGGGGTACCTATTATTTGAAGGTATATCCAATG (reverse-H). The PCR products consisting of the native subunit C and H sequences capped by the cloning restriction sites were first subcloned into a modified pET expression vector (pETM-11) using the NcoI and Acc65I sites (underlined in the sequences given above) and further cloned into the pET3d vector at the NcoI and BamHI sites. The latter vector has an ampicillin resistance gene, which is necessary for selection of the right transformants in the coexpression experiments. The identity of the cloned products was confirmed by sequencing. Subunits E and G were cloned into a kanamycin bicistronic vector as described previously (*35*) with subunit G carrying an N-terminal six-His tag. They were also separately cloned into the pET3d ampicillin vector from the pETM41 kanamycin vector (*35*). Formation of the complexes was achieved by cotransforming electrocompetent *Escherichia coli* BL-21 (DE3) cells with different vector combinations to investigate the specificity of the interactions, and plating onto LB agar supplemented with kanamycin (30 μg/mL) and ampicillin (100 μg/mL). For 2 L expression of the complexes, 4 mL of SOC medium containing 50 μg/mL kanamycin, 200 μg/mL carbenicillin, and 1% glucose was inoculated with a single colony and grown overnight at 37 °C. The next day, 2 mL of this culture was transferred into 500 mL of TB medium containing 50 μg/mL kanamycin, 200 μg/mL carbenicillin, and 1% glucose, and grown at 37 °C. When the OD_{600} reached 0.7, 0.2 mM IPTG was added and expression was carried out for 16−20 h at room temperature in Innova shakers at 250 rpm.

Purification Procedure. After expression, cells (20−30 g wet weight) were centrifuged for 10 min at 4000*g* and resuspended in 4 mL of buffer A [50 mM Tris-HCl (pH 8.0), 0.3 M NaCl, 1 mM $MgCl_2$, 1 mM PMSF, and one tablet/100 mL of complete EDTA-free protease inhibitors from Roche Applied Sciences] per gram of cells for lysis in the Avestin Emulsiflex-C5 emulsifier. The lysed cells were centrifuged at 200000*g* for 60 min, and recombinant proteins in the supernatant (separated in 60 mL aliquots) were purified by metal chelating affinity chromatography. A 7.8 mL POROS MC20 perfusion column with Ni^{2+} as the chelating metal was pre-equilibrated with buffer B [50 mM Tris-HCl (pH 8.0), 0.3 M NaCl, 1 mM PMSF, and one tablet/100 mL of complete EDTA-free protease inhibitor], and the sample was loaded at 5 mL/min. After an extensive washing of the column with buffer B, the protein was eluted with a 0 to 0.5 M imidazole gradient in 10 column volumes (in buffer B), and fractions (5 mL) were analyzed by gel electrophoresis. In experiments in which the subunits copurified due to their specific interaction, the eluting fractions were pooled (100−150 mL depending on the complex) and dialyzed against 2 × 2 L of buffer C [50 mM Tris-HCl (pH 8.0)]. The sample was further diluted 2-fold with buffer C and loaded on an anion exchange perfusion column (POROS HQ20) pre-equilibrated with buffer C. After being extensively washed, the protein complex was eluted with a sharp NaCl gradient in buffer C. Fractions were pooled (15−20 mL), concentrated to 0.5−1 mL, and loaded on a preparative scale high-resolution Superdex-200 gel filtration column equilibrated in buffer D [20 mM Tris-HCl (pH 8.0), 150 mM NaCl, 1 mM PMSF, and 1 tablet/100 mL of complete EDTA-free protease inhibitors]. Fractions were analyzed by SDS−

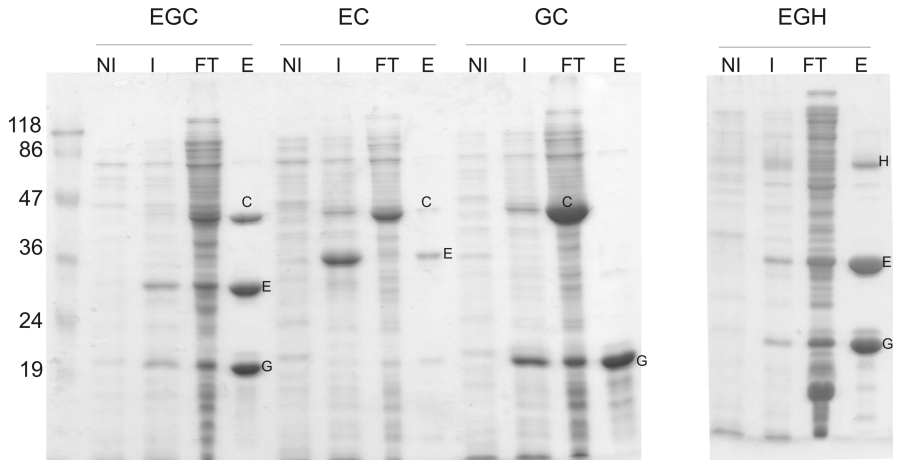

FIGURE 1: Overexpression of EGC, EC, GC, and EGH complexes in *E. coli*. NI represents noninduced, I induced, FT the flow-through from the Ni^{2+} column, and E the elution from the Ni^{2+} column. Cells were cultured, and expression was induced as described in Experimental Procedures. Aliquots of each sample were analyzed on a 15% SDS gel, and stained with Coomassie blue; 5 μL of cells (NI and I lanes) or of the pooled fractions (FT and E lanes) was loaded onto the gel. The different migration of subunit E in the various subcomplexes is due to the presence or absence of the His tag.

PAGE, and concentrated by ultrafiltration on Amicon ultra YM30 or YM10 membranes (Millipore) to a concentration of 5−10 mg/mL. Protein concentration was determined with the BCA assay (Pierce). From 2 L cultures, 3−5 mg of pure protein could be obtained. Native masses (M) were calculated from the Svedberg equation:

$$M = \frac{sRT}{D(1 - \bar{v}\rho)}$$

where s is the sedimentation coefficient obtained from the analytical centrifugation, R is the gas constant (8.314 J K^{-1} mol^{-1}), T is the temperature in kelvin, D is the diffusion coefficient estimated from the size exclusion chromatography data, $\bar{v}$ is the partial specific volume calculated from the amino acid sequence, and ρ is the solvent density.

Analytical Ultracentrifugation. The samples eluting from the gel filtration column were concentrated and/or dialyzed to an A_{280} of ~0.4−0.5 in 5−20 mM Tris-HCl (pH 8) and 150 mM NaCl and used directly for sedimentation velocity and equilibrium analytical ultracentrifugation at 20 °C in a Beckman ProteomeLab XL-A centrifuge equipped with an AN-60 rotor and absorbance optics. Sedimentation velocity experiments were performed at a speed of 50 000 (EG) or 40 000 rpm (EGC). Absorbance scans were taken at 280 nm at 1.5 (EG) or 3.5 min (EGC) intervals, with a 0.003 cm radial scan step. Sedimentation equilibrium data were recorded at speeds of 10 000, 14 000, and 20 000 rpm at 1 h intervals with a 0.001 cm step size and five replicates per data point. Six-sector cells were loaded from low to high radius with 1-, 2-, and 4-fold dilutions of the ~0.45A_{280} stock solutions, corresponding approximately to 36, 18, and 9 μM (EG) or 9, 4.5, and 2.25 μM (EGC), respectively.

The protein partial specific volume ($\bar{v}$), buffer density (ρ), and viscosity (η) were calculated using SEDNTERP[2] (*36*). Since the stoichiometry of the complexes was initially uncertain, data were processed using the slightly different values of $\bar{v}$ calculated for complexes of EG and EG_2, or EGC and EG_2C. No significant differences were observed in the results obtained, all of which were consistent with the 1:1(:1) stoichiometry used for final analysis. Sedimentation coefficient distributions and weight-averaged frictional ratios were calculated using SEDFIT87 (*37*). Sedimentation equilibrium data were initially processed using WINNONLIN version 1.06 (*38*) assuming the presence of a single species. To assess the existence of possible equilibria among multiple components, data were further analyzed using SEDANAL version 3.61 (*39*).

Native PAGE and SDS−PAGE. Native gel electrophoresis was performed with the Novex gel system according to the manufacturer's recommendations. The pure concentrated complexes were mixed 1:1 with the tris-glycine native loading buffer, and loaded on an 8−16% tris-glycine gel. Electrophoresis was carried out at 4 °C for 3.0 h. The gel was stained with Coomassie blue R250. The native complexes were analyzed in a second denaturing dimension. Bands corresponding to the respective complexes were excised from the native gel, minced, and incubated in 2 mL of SDS sample buffer overnight at room temperature for elution. The samples were then concentrated on a microcon concentrator with a 10 kDa cutoff before being loaded on the denaturing gel. SDS−PAGE was performed according to the method of Laemmli (*40*).

RESULTS

Coexpression and Purification. Subunits E and G were coexpressed from a bicistronic vector together with subunit C or H in BL21(DE3) cells at room temperature. To ensure stability of the plasmid carrying subunit C or H, carbenicillin was used at 200 μg/mL during preculture and supplemented prior to induction to maintain selection pressure. This was apparently not sufficient to avoid a lower level of expression from the ampicillin plasmids. As can be seen in the EGC portion of Figure 1, subunits E and G are clearly detectable in the cell culture after induction for 20 h whereas subunit C is barely visible before purification. This effect is also apparent for the other dual-vector expression (Figure 1, EC and GC), but to a lesser extent for EGH. Nevertheless, all proteins accumulated in the cell as soluble entities, and specific complexes could be isolated by copurification on metal-chelating affinity chromatography support (Figure 1).

[2] J. Philo, D. Hayes, and T. Laue, unpublished observations.

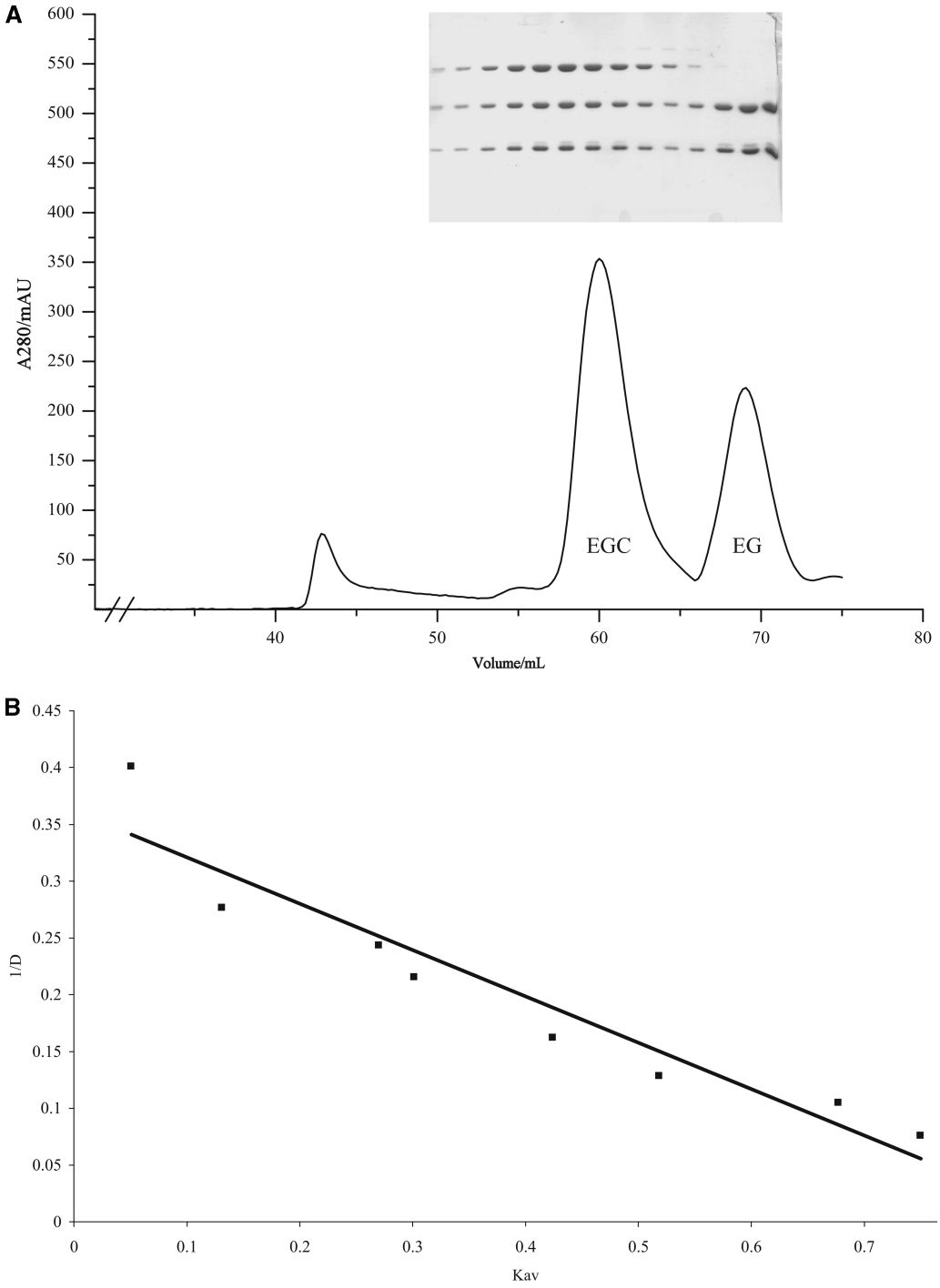

FIGURE 2: (A) High-resolution gel filtration separation of EGC and EG complexes. Copurified complexes were concentrated to 1 mL and loaded on a 120 mL Superdex-200 preparative size exclusion chromatography column (A). Fractions were analyzed by SDS−PAGE (inset). (B) Calibration of the column was based on the diffusion coefficient of a series of globular proteins with their inverse diffusion coefficients (1/*D*) plotted as a function of their partition coefficients (K_{av}).

The purification was achieved with a combination of Ni^{2+} affinity chromatography, ion exchange, and gel filtration. In all cases, the smallest subunits, G or E, depending on the coexpression partner, carried the histidine tag. For the EGC or EGH complexes, all three proteins eluted from the Ni^{2+} affinity column as single peaks, indicating their specific interaction (Figure 1, elution). The intrinsic specificity of the EGC interaction was investigated by coexpressing different combinations of the subunits in a dual-plasmid configuration, while changing the histidine-tagged partners. When subunit E carrying the tag is coexpressed with native subunit C, a substantial amount of the latter flows through the Ni^{2+} column. However, a faint band corresponding to subunit C can be detected in the elution peak, together with subunit E (Figure 1, EC). In this complex, because of the tag, subunit E migrates with a higher apparent molecular mass. On the other hand, a similar combination of native subunit C with His-tagged subunit G shows subunit G eluting as a single entity from the Ni^{2+} column while subunit C is found exclusively in the flow-through (Figure 1, GC).

As was previously observed with the pETM11-EG bicistronic vector in coexpression experiments (*35*) and as discussed above, different levels of expression are observed for the different proteins, with the one carrying the histidine

Table 1: Hydrodynamic Properties of the Stator Subunits of the Yeast V-ATPase[a]

	K_{av}	M_r(SEC) (K_{av} vs M_r)	$D_{20,w}$(SEC) (K_{av} vs 1/D) ($\times 10^7$ cm^2 s^{-1})	s ($\times 10^{-13}$)	M_r (Svedberg)	M_r(Eq.Sed.)	M_r(calcd)
scEG	0.379	107 000	4.86	2.26	44 735	44 100	42 669
scEGC	0.252	216 000	3.88	3.32	82 401	83 456	86 851

[a] K_{av} values were obtained from elution volumes from size exclusion chromatography (SEC) experiments. $D_{20,w}$ is the diffusional coefficient estimated from the calibration of the size exclusion chromatography column. s is the sedimentation coefficient obtained from velocity centrifugation analysis. M_r represents the molecular mass in daltons estimated from the different techniques [SEC, Svedberg equation, equilibrium sedimentation (Eq.Sed.)]. The calculated M_r was estimated from the cloned sequences of the different subunits, assuming a 1:1(:1) stoichiometry.

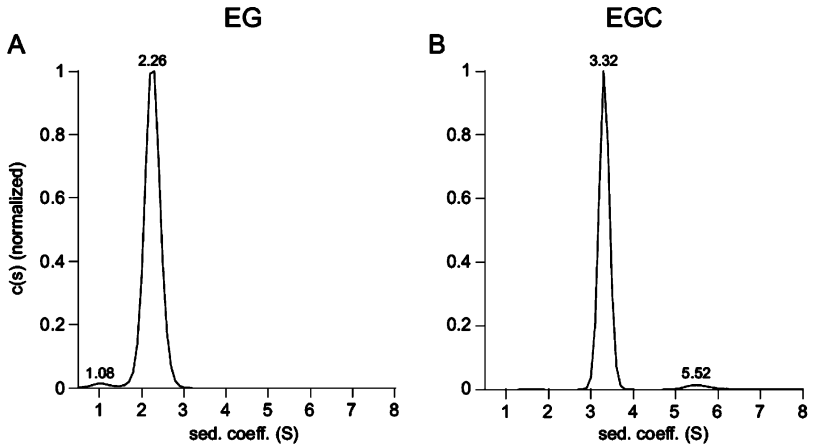

FIGURE 3: Hydrodynamic characterization of EG and EGC complexes. Sedimentation velocity experiments were performed on SEC-purified complexes at 20 °C. The sedimentation coefficient distributions are shown for the EG (A) and EGC (B) complexes, together with the positions of observed peaks. The main peaks account for >95% of the material detected. Similarly large weight-averaged frictional coefficients were obtained for both complexes so that the difference in sedimentation behavior primarily reflects the size difference between them.

tag often expressed at higher levels. This may lead to the formation of different subcomplexes with varying stoichiometries. In the case presented here, because of the smaller amount of subunit C that is produced, an excess of the EG complex together with free subunit G will not be involved in complex formation and contaminate the preparation. These were separated by ion exchange and high-resolution size exclusion chromatography. Free subunit G, because of its high pI, does not bind to the anion exchange column at the pH used, and can be separated from the remaining complexes. The EGC and excess EG complexes are well resolved from one another and elute as single peaks from the gel filtration column with elution volumes corresponding to very large complexes (Figure 2A). The inset in Figure 2A shows the gel of the eluting fractions, and indicates the high resolving power of the separation allowing very pure EGC and EG complexes to be isolated. The EGH complex eluted from the gel filtration column as a single peak, but much earlier than the EGC complex, with almost no free EG complex (data not shown). Because it has been proposed that two isoforms of subunit H might be bound to the V-ATPase complex (*24*), the gel filtration data were not immediately dismissed as aggregates, and the complex was analyzed by sedimentation velocity ultracentrifugation. Unfortunately, although the sample did exhibit a species sedimenting at ~3.2 S (which would correlate with a 1:1:1 complex), it is clearly not homogeneous, and sedimentation equilibrium analysis was not attempted.

We have also investigated the ability of the subunits to associate in vitro to form the ternary complex. In contrast to the EG complex, which cannot associate in vitro (*35*), we were able to recreate the EGC complex from an equimolar combination of pure recombinant subunit C and EG complex. The resulting de novo complex eluted as a single peak on the gel filtration column at the exact elution volume of the EGC complex resulting from the coexpression of the individual subunits (data not shown). Because of the suspected aggregation of subunit H, this in vitro reconstitution was not attempted for the EGH complex.

Hydrodynamic Properties of the EG and EGC Complexes. Although the EG and EGC complexes eluted from the size exclusion column as single symmetric peaks, the molecular masses calculated using globular protein markers (Table 1) are likely to be influenced by the shape of the stator subcomplexes. From our previous study on the EG complex (*35*) and the crystal structure of subunit C (*30*), it is expected that the complexes are elongated, which would cause anomalously early elution during SEC. To determine a more accurate native molecular mass and assess the species homogeneity in our preparations, we have further characterized the hydrodynamic properties of these complexes by analytical ultracentrifugation.

The sedimentation velocity experiment with the EG complex yields a distribution of sedimentation coefficients with a single prominent peak at 2.26 S (98% of the signal at >0.5 S), and a minor secondary peak at 1.08 S (2%) (Figure 3A). The $c(s)$ distribution for the EGC complex also exhibits a single prominent peak at 3.32 S (95%), again with a minor secondary peak, in this case at a higher sedimentation coefficient (5.52 S; 3%) (Figure 3B). In both cases, as expected, the frictional ratio indicates an elongated structure ($f/f_0 = 1.52$ and 1.74 for EG and EGC, respectively). Since

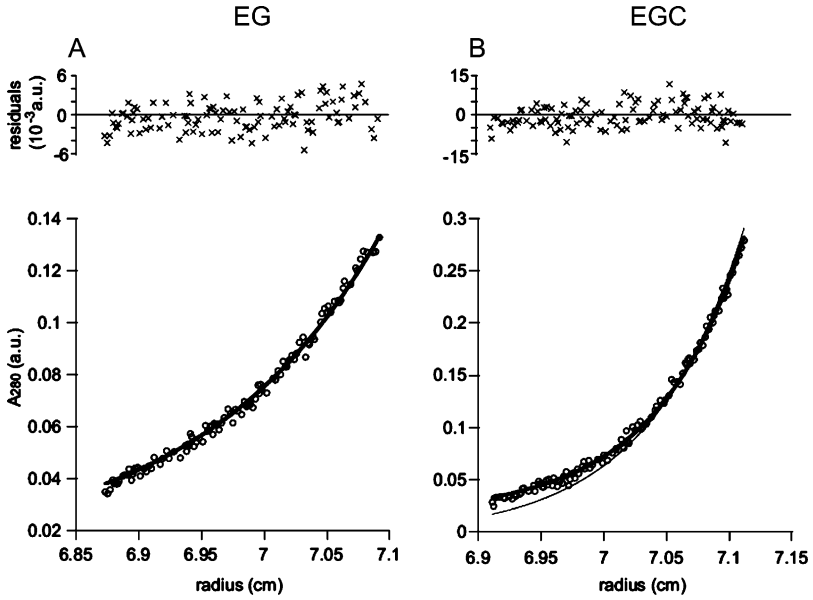

FIGURE 4: Molecular mass and stoichiometry of the EG and EGC complexes. Sedimentation equilibrium data are shown for the EG (A) and EGC (B) complexes. Data were fit globally (three speeds and three concentrations) but are shown for only a single curve (14 000 rpm, outermost chamber, starting protein concentrations of ~9 and ~2.25 μM for the EG and EGC complexes, respectively). Calculated fits are shown as thick lines for a single species (EG) and for two noninteracting species (EGC), and the corresponding residuals are shown at the top. Each fit is consistent with a 1:1 or 1:1:1 stoichiometry. The single-species fit is shown for EGC as a thin line.

calibration of SEC data (K_{av}) against ln(M_r) is valid only for proteins similar in shape to the (globular) standards that were used, it is clearly inappropriate for the stator complexes. The more fundamental (i.e., shape-independent) correlation is between K_{av} and the inverse diffusion coefficient $1/D_{20,w}$ (Figure 2B). When recalibrated in this way, the SEC data yield $D_{20,w}$ estimates for the EG and EGC complexes of 4.86 $\times$ 10^{-7} and 3.88 $\times$ 10^{-7} cm^2/s, respectively (Table 1). By combining these data with the sedimentation coefficients described above, we obtain M_r values for EG and EGC complexes of 44.7 and 82.4 kDa, respectively, consistent with the assembly of one subunit each in a 1:1(:1) stoichiometry (Table 1). Repeated measurements of the EG complex reveal sedimentation coefficients clustered within 0.05 S (n = 3), corresponding to approximately $\pm$1 kDa in the Svedberg equation. For the EGC complex, the fit performed in the absence of regularization provides a similar estimate of the standard deviation of s of 0.054 S.

The sedimentation equilibrium experiments confirm these estimates. For the EG complex, the multispeed data at three concentrations can be well fit globally by a single-species model, where M_r = 44.1 kDa (rmsd = 0.0036), consistent with a 1:1 complex (Figure 4A). Given the presence of the small secondary peak in the $c(s)$ distribution (Figure 3A), the equilibrium data were also fit assuming different bimolecular interactions (E + G = EG or EG + G = EGG). Only slight improvements were observed in the resulting fits (rmsd = 0.0035 or 0.0034, respectively), most likely reflecting the increased number of free parameters, rather than the presence of significant populations of additional molecular species.

For the EGC complex, sedimentation equilibrium data fit globally with a single-species model yield an M_r estimate of 83.5 kDa (rmsd = 0.007; Figure 4B, thin line), but exhibit systematic residuals that suggest the presence of additional species. As suggested by the $c(s)$ distribution (Figure 3B), a significantly improved fit (rmsd = 0.0048; Figure 4B, thick line and residual plot) is obtained by assuming the presence of a second, noninteracting species with a larger M_r, in addition to the dominant component with M_r fixed at the calculated value for a 1:1:1 EGC complex (86.8 kDa). The amount of contaminant refines to a value ~2−5% of the EGC concentration, again consistent with the $c(s)$ distribution. No equivalent or better fit was obtained by assuming the existence of equilibria involving either the partial dissociation of the EGC complex or the association of additional subunits with it.

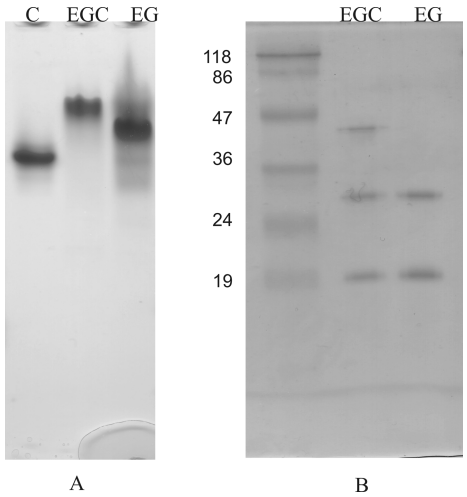

FIGURE 5: Polyacrylamide gel electrophoresis analysis of the EGC and EG complexes: (A) 8−16% Tris-glycine native gel of pure subunit C, the EGC complex, and the EG complex and (B) 15% SDS−PAGE of the EGC and EG complexes eluted from the native gel in panel A.

Homogeneity of the Complex (Native Gel of the Complex). The integrity of the trimeric EGC complexes was verified by native gel electrophoresis. Figure 5A clearly shows the formation of the stoichiometric complexes. In comparison to subunit C alone or the EG complex, the migration of the EGC complex is significantly retarded, indicating its larger

mass. In addition, no individual subunits, other subcomplexes, or larger oligomers are detected on the gel. The band shift observed in relation to subunit C alone or the EG complex supports unequivocally the formation of specific EGC complexes. The composition of these native complexes was further confirmed by SDS−PAGE. Bands corresponding to the EG and EGC complexes were excised from the native gel and analyzed on a second dimension under denaturing conditions. Figure 5B shows the expected composition of the respective bands with the EG and the EGC complexes being dissociated into their respective components on the denaturing gel, which further supports the results obtained under native conditions.

DISCUSSION

Specific Subunit Interactions. In this report, we have further pursued our effort to investigate the physical interactions between stator subunits of the yeast V-ATPase to refine our topological characterization of the enzyme, and provide a more accurate model of this unique domain. The coexpression strategy proved to be very efficient in our first study of the EG complex and has now been extended further for the reconstruction of an isolated recombinant stator complex structure containing subunit C. Several earlier pieces of evidence (*18*, *20*), together with the recently determined structure of yeast subunit C (*30*), and the three-dimensional reconstructions of the intact enzyme (*24*, *28*, *29*), have suggested that this subunit C may have a role as a stator subunit and participate in the attachment of V_1 to V_0. Its extended helical structure together with its proposed role in the regulation of the enzyme by reversible dissociation (*10*, *13*, *41*) prompted us to use our strategy to investigate more thoroughly the nature and stoichiometry of its interactions with other proposed stator subunits. This has some functional importance, as subunit C is known to be an intermediate in the metabolic regulation of the enzyme, through subunit dissociation.

Our data show that subunits E, G, and C form a ternary complex. The velocity centrifugation analysis of both the EG and EGC complexes indicates an elongated conformation corresponding to the predicted structures of the E and G subunits, the EM structure of their complex (*35*), and the X-ray structure of subunit C (*30*). Here, we have been able to create this complex in vitro, by combining the C subunit with the preformed EG complex.

In contrast, subunit G alone does not interact with subunit C. No copurification of a CG complex was obtained with our strategy. Indeed, precipitation assays (*42*) as well as cross-linking experiments (*17*) show no evidence for GC interaction. These data indicate that the EGC complex does not form exclusively through a pathway involving the interaction of subunit C with subunit G. Similarly, very little subunit C copurifies with subunit E, and no stable EC complex could be unambiguously isolated. We believe that these observations are most consistent with a lack of stability of the EC complex, which may not survive the multiple purification steps under nonequilibrium conditions. In contrast, the interaction can be detected in fully assembled complexes by cross-linking (*17*) assays, and in vitro by comparatively rapid immunoprecipitation methods (*18*, *42*).

Taken together, our data suggest that the EG complex may represent a stable core that serves as a template for the assembly of other subunits in the formation of a functional stator. Not only does EG interact more strongly with C than does either the E or G subunit alone, but the formation of the EG complex appears to stabilize both of the components. In our system, subunit G appears to have a non-native conformation in the absence of subunit E, and probably requires interaction with subunit E for complete folding (*35*). Conversely, it has been reported that there is a lack of stability of subunit E in the absence of subunit G in vivo (*20*).

Once the complex is assembled, we find that the EG core can interact not only with subunit C but also with subunit H. The resulting EGH complex elutes as a single peak from the size exclusion chromatography column, but given the heterogeneity seen in sedimentation velocity experiments, further studies will be required to establish an unambiguous stoichiometry. Previously, precipitation as well as two-hybrid and cross-linking assays (*17*, *22*) have revealed interaction between subunits E and H. Because of the extensive aggregation of subunit H, we were not been able to verify the specificity of the EGH interaction, but believe that as in the case of the EGC complex, EG must form before the addition of subunit H, suggesting an assembly pathway similar to that of the EGC complex. Interaction of subunit H with the membrane-bound subunit *a* (*43*) would then provide an anchor for a potential separate EGH*a* stator domain.

It has long been recognized that V-ATPases share a common architecture with the F-ATPases, especially in the subunit composition of the catalytic rotor domain. In each of the respective complexes, the F-ATPase subunits have their equivalent counterparts in the V-ATPases. However, several additional polypeptide chains in the V-ATPase are unique, and are believed to contribute to the formation of a peripheral stator that is much more complex than that of the F-ATPases. We and others have already shown that subunits E and G form a complex to fulfill a similar function as the *b* stator in F-ATPase. The soluble domain of the latter is known to be dimeric (*44*). On the basis of amino acid analysis, it has been proposed that two copies of subunit G are present per complex (*17*), and a recombinant form of this subunit has been shown to form a dimer in solution through its N-terminus (*33*). These data support the homology of part of the V-ATPase stator to the dimeric *b* stator structure of F-ATPases. However, considering the aforementioned complexity of this region in V-ATPases, it is clear that additional subunits must participate in this stator. Several studies have reported the in vivo isolation of subcomplexes of the yeast V-ATPase (*19*, *20*, *23*) as well as in vitro interactions (*17*, *18*, *21*, *22*, *42*, *43*). Some of these studies have permitted the identification of stator subcomplexes. However, a clear physical interaction between the different isolated partners has never been demonstrated.

We believe that the strategy of coexpression and purification of defined homogeneous subcomplexes is a good complement to co-immunoprecipitation studies, providing support for the existence of these interactions. In addition, this strategy permits the isolation of large quantities of these complexes for further biophysical characterization and structural studies. In its current design, namely, an isolated recombinant system, this strategy is providing the first clear evidence of direct physical interaction and of the stoichi-

ometry of the interacting subunits of the stator of the yeast V-ATPase. Because of the elongated shape of most of the subunits forming the stator (*30*, *33*, *35*, *45*), gel filtration analysis cannot provide a reliable estimation of the mass of the complexes. However, by measuring sedimentation coefficients and combining the values with the gel filtration data by means of the Svedberg equation, we can calculate shape-independent estimates of these masses. These are confirmed by sedimentation equilibrium analysis. Taken together, the most parsimonious explanation for our sedimentation velocity and equilibrium data is that at the concentrations used in these experiments (~2−40 μM), the predominant species in solution are EG or EGC complexes containing each component in a 1:1(:1) stoichiometry.

The fact that no EG_2 or EG_2C complexes were detected does not necessarily conflict with previous reports (*33*). Addition of a second G subunit would shift the observed masses by 16 kDa, a value much higher than the error in measurement. It was also not possible to detect the formation of significant amounts of G2 complexes by fitting the sedimentation equilibrium data by multistep associative models. However, the 1:1(:1) stoichiometry was detected at a particular protein concentration, and it is possible that a lower-affinity binding site for a second G subunit exists but was not occupied. Furthermore, it is possible that binding of a second G subunit could be stabilized within the context of a fully assembled V-ATPase by interactions with other subunits. Nevertheless, our data clearly establish the biochemical interactions that characterize the minimal assembly competent stator core.

It has been reported that the isolated G subunit can form dimers in solution (*33*). However, in our hands, isolated subunit G has a strong tendency to aggregate and a high susceptibility to proteolytic degradation. Previous reports have also shown that the isolated G subunit is not well-folded (*34*, *35*, *46*, *47*), nor has a G dimer been detected in cross-linking studies (*17*). As an alternative, on the basis of the data presented here, we propose that the fundamental stator assembly step is the association of a single E and a single G subunit. In particular, we have demonstrated that the 1:1 EG complex is able to bind either C or H subunits when coexpressed, and can be reconstituted with equimolar amounts of purified C subunit in vitro. On the basis of the 3D EM models of related V-ATPases in which extensive densities are seen on both sides of the catalytic V_1 (*24*, *29*, *48*), it is tempting to speculate about the existence of a second EG complex. According to our current results, one could imagine on one side an EGC stator and on the other an EGH stator, both interacting with the N-terminus of subunit *a* providing the membrane anchor. However, this would require two E subunits as well, which is possible (*19*, *31*) but controversial (*32*).

In this report, we present data in an attempt to complete the construction of a recombinant stator for the yeast V-ATPase. Using a coexpression strategy, we have isolated a stoichiometric EGC complex and confirmed the stoichiometry of a previously isolated EG complex. Specific interaction between the EG complex and subunit H has also been demonstrated. Together, these data pave the way to the isolation of a complete recombinant stator for the V-ATPase as well as an intact recombinant V_1 domain, which will permit more detailed biochemical and biophysical investigations. In addition, this strategy gives the possibility of isolating defined subcomplexes for further structural characterization, which could lead to a better interpretation of models derived from electron microscopy analysis.

ACKNOWLEDGMENT

We thank Dr. T. Laue (University of New Hampshire, Durham, NH) for helpful suggestions and Dr. H. Higgs (Dartmouth Medical School) for assistance with the analytical ultracentrifugation.

REFERENCES

1. Madshus, I. G. (1988) Regulation of intracellular pH in eukaryotic cells, *Biochem. J. 250*, 1−8.
2. Stevens, T. H., and Forgac, M. (1997) Structure, function and regulation of the vacuolar H^+-ATPase, *Annu. Rev. Cell Dev. Biol. 13*, 779−808.
3. Nishi, T., and Forgac, M. (2002) The vacuolar H^+-ATPases: Nature's most versatile proton pumps, *Nat. Rev. Mol. Cell Biol. 3*, 94−103.
4. Futai, M., Oka, T., Sun-Wada, G., Moriyama, Y., Kanazawa, H., and Wada, Y. (2000) Luminal acidification of diverse organelles by V-ATPase in animal cells, *J. Exp. Biol. 203*, 107−116.
5. Gluck, S. L. (1992) The structure and biochemistry of the vacuolar H^+ ATPase in proximal and distal urinary acidification, *J. Bioenerg. Biomembr. 24*, 351−359.
6. Swallow, C. J., Grinstein, S., and Rotstein, O. D. (1990) A vacuolar type H^+-ATPase regulates cytoplasmic pH in murine macrophages, *J. Biol. Chem. 265*, 7645−7654.
7. Chatterjee, D., Chakraborty, M., Leit, M., Neff, L., Jamsa-Kellokumpu, S., Fuchs, R., and Baron, R. (1992) Sensitivity to vanadate and isoforms of subunits A and B distinguish the osteoclast proton pump from other vacuolar H^+ ATPases, *Proc. Natl. Acad. Sci. U.S.A. 89*, 6257−6261.
8. Martinez-Zaguilan, R., Lynch, R. M., Martinez, G. M., and Gillies, R. J. (1993) Vacuolar-type H^+-ATPases are functionally expressed in plasma membranes of human tumor cells, *Am. J. Physiol. 265*, C1015−C1029.
9. Bowman, B. J., Dschida, W. J., Harris, T., and Bowman, E. J. (1989) The vacuolar ATPase of *Neurospora crassa* contains an F1-like structure, *J. Biol. Chem. 264*, 15606−15612.
10. Kane, P. M. (1995) Disassembly and reassembly of the yeast vacuolar H^+-ATPase *in vivo*, *J. Biol. Chem. 270*, 17025−17032.
11. Kane, P. M., and Smardon, A. M. (2003) Assembly and regulation of the yeast vacuolar H^+-ATPase, *J. Bioenerg. Biomembr. 35*, 313−321.
12. Kane, P. M., and Parra, K. J. (2000) Assembly and regulation of the yeast vacuolar H^+-ATPase, *J. Exp. Biol. 203*, 81−87.
13. Sumner, J. P., Dow, J. A. T., Earley, F. G. P., Klein, U., Jäger, D., and Wieczorek, H. (1995) Regulation of plasma membrane V-ATPase activity by dissociation of peripheral subunits, *J. Biol. Chem. 270*, 5649−5653.
14. Rubinstein, J. L., Walker, J. E., and Henderson, R. (2003) Structure of the mitochondrial ATP synthase by electron cryomicroscopy, *EMBO J. 22*, 6182−6192.
15. Wilkens, S., and Capaldi, R. A. (1998) ATP synthase's second stalk comes into focus, *Nature 393*, 29.
16. Mellwig, C., and Böttcher, B. (2003) A unique resting position of the ATP-synthase from chloroplasts, *J. Biol. Chem. 278*, 18544−18549.
17. Xu, T., Vasilyeva, E., and Forgac, M. (1999) Subunit interactions in the clathrin-coated vesicle vacuolar H^+-ATPase Complex, *J. Biol. Chem. 274*, 28909−28915.
18. Puopolo, K., Sczekan, M., Magner, R., and Forgac, M. (1992) The 40-kDa subunit enhances but is not required for activity of the coated vesicle proton pump, *J. Biol. Chem. 267*, 5171−5176.
19. Tomashek, J. J., Sonnenburg, J. L., Artimovich, J. M., and Klionsky, D. J. (1996) Resolution of subunit interactions and cytoplasmic subcomplexes of the yeast vacuolar proton-translocating ATPase, *J. Biol. Chem. 271*, 10397−10404.
20. Tomashek, J. J., Garrison, B. S., and Klionsky, D. J. (1997) Reconstitution in Vitro of the V1 Complex from the Yeast Vacuolar Proton-translocating ATPase. Assembly recapitulates mechanism, *J. Biol. Chem. 272*, 16618−16623.

21. Arata, Y., Baleja, J. D., and Forgac, M. (2002) Localization of subunits D, E, and G in the yeast V-ATPase complex using cysteine-mediated cross-linking to subunit B, *Biochemistry 41*, 11301−11307.
22. Lu, M., Vergara, S., Zhang, L., Holliday, L. S., Aris, J., and Gluck, S. L. (2002) The Amino-terminal Domain of the E Subunit of Vacuolar H^+-ATPase (V-ATPase) Interacts with the H Subunit and Is Required for V-ATPase Function, *J. Biol. Chem. 277*, 38409−38415.
23. Tomashek, J. J., Graham, L. A., Hutchins, M. U., Stevens, T. H., and Klionsky, D. J. (1997) V1-situated Stalk Subunits of the Yeast Vacuolar Proton-translocating ATPase, *J. Biol. Chem. 272*, 26787−26793.
24. Wilkens, S., Inoue, T., and Forgac, M. (2004) Three-Dimensional structure of the vacuolar ATPase: Localization of subunit H by difference imaging and chemical cross-linking, *J. Biol. Chem. 279*, 41942−41949.
25. Wilkens, S., Vasilyeva, E., and Forgac, M. (1999) Structure of the vacuolar ATPase by electron microscopy, *J. Biol. Chem. 274*, 31804−31810.
26. Grüber, G., Radermacher, M., Ruiz, T., Godovac-Zimmermann, J., Canas, B., Kleine-Kohlbrecher, D., Huss, M., Harvey, W. R., and Wieczorek, H. (2000) Three-dimensional structure and subunit topology of the V_1 ATPase from *Manduca sexta* midgut, *Biochemistry 39*, 8609−8616.
27. Rizzo, V. F., Coskun, U., Radermacher, M., Ruiz, T., Armbrüster, A., and Grüber, G. (2003) Resolution of the V1 ATPase from *Manduca sexta* into subcomplexes and visualization of an ATPase-active A3B3EG complex by electron microscopy, *J. Biol. Chem. 278*, 270−275.
28. Domgall, I., Venzke, D., Lüttge, U., Ratajczak, R., and Böttcher, B. (2002) Three-dimensional map of a plant V-ATPase based on electron microscopy, *J. Biol. Chem. 277*, 13115−13121.
29. Venzke, D., Domgall, I., Köcher, T., Féthière, J., Fischer, S., and Böttcher, B. (2005) Elucidation of the Stator Organization in the V-ATPase of *Neurospora crassa*, *J. Mol. Biol. 349*, 659−669.
30. Drory, O., Frolow, F., and Nelson, N. (2004) Crystal structure of yeast V-ATPase subunit C reveals its stator function, *EMBO Rep. 5*, 1148−1152.
31. Xie, X. S. (1996) Reconstitution of ATPase Activity from Individual Subunits of the Clathrin-coated Vesicle Proton Pump. The requirement and effect of three small subunits, *J. Biol. Chem. 271*, 30980−30985.
32. Arai, H., Terres, G., Pink, S., and Forgac, M. (1988) Topography and subunit stoichiometry of the coated vesicle proton pump, *J. Biol. Chem. 263*, 8796−8802.
33. Armbrüster, A., Bailer, S. M., Koch, M. H. J., Godovac-Zimmermann, J., and Grüber, G. (2003) Dimer formation of subunit G of the yeast V-ATPase, *FEBS Lett. 546*, 395−400.
34. Crider, B. P., Andersen, P., White, A. E., Zhou, Z., Li, X., Mattsson, J. P., Lundberg, L., Keeling, D. J., Xie, X. S., Stone, D. K., and Peng, S. B. (1997) Subunit G of the vacuolar proton pump. Molecular characterization and functional expression, *J. Biol. Chem. 272*, 10721−10728.
35. Féthière, J., Venzke, D., Diepholz, M., Seybert, A., Geerlof, A., Gentzel, M., Wilm, M., and Böttcher, B. (2004) Building the Stator of the Yeast Vacuolar-ATPase: Specific interaction between subunits E and G, *J. Biol. Chem. 279*, 40670−40676.
36. Laue, T. M., Shah, B. D., Ridgeway, T. M., and Pelletier, S. L. (1992) Computer-aided interpretation of analytical sedimentation data for proteins, in *Analytical Ultracentrifugation in Biochemistry and Polymer Sciences* (Harding, S. E., Rowe, A. J., and Horton, J. C., Eds.) pp 90−125, Royal Society for Chemistry, Cambridge, U.K.
37. Dam, J., and Schuck, P. (2004) Calculating sedimentation coefficient distributions by direct modeling of sedimentation velocity concentration profiles, *Methods Enzymol. 384*, 185−212.
38. Johnson, M. L., Correia, J. J., Yphantis, D. A., and Halvorson, H. R. (1981) Analysis of data from the analytical ultracentrifuge by nonlinear least-squares techniques, *Biophys. J. 36*, 575−588.
39. Stafford, W. F., and Sherwood, P. J. (2004) Analysis of heterologous interacting systems by sedimentation velocity: Curve fitting algorithms for estimation of sedimentation coefficients, equilibrium and kinetic constants, *Biophys. Chem. 108*, 231−243.
40. Laemmli, U. K. (1970) Cleavage of structural proteins during the assembly of the head of bacteriophage T4, *Nature 227*, 680−685.
41. Doherty, R. D., and Kane, P. M. (1993) Partial assembly of the yeast vacuolar H^+-ATPase in mutants lacking one subunit of the enzyme, *J. Biol. Chem. 268*, 16845−16851.
42. Jones, R. P. O., Durose, L. J., Findlay, J. B. C., and Harrison, M. A. (2005) Defined sites of interaction between subunits E (Vma4p), C (Vma5p), and G (Vma10p) within the stator structure of the vacuolar H^+-ATPase, *Biochemistry 44*, 3933−3941.
43. Landolt-Marticorena, C., Williams, K. M., Correa, J., Chen, W., and Manolson, M. F. (2000) Evidence that the NH2 terminus of Vph1p, an integral subunit of the V0 sector of the yeast V-ATPase, interacts directly with the Vma1p and Vma13p subunits of the V1 sector, *J. Biol. Chem. 275*, 15449−15457.
44. Dunn, S. D. (1992) The polar domain of the b subunit of *Escherichia coli* F_1F_0-ATPase forms an elongated dimer that interacts with the F1 sector, *J. Biol. Chem. 267*, 7630−7636.
45. Sagermann, M., Stevens, T. H., and Matthews, B. W. (2001) Crystal structure of the regulatory subunit H of the V-type ATPase of *Saccharomyces cerevisiae*, *Proc. Natl. Acad. Sci. U.S.A. 98*, 7134−7139.
46. Harrison, M., Durose, L., Song, C. F., Barratt, E., Trinick, J., Jones, R., and Findlay, J. B. (2003) Structure and function of the vacuolar H^+-ATPase: Moving from low-resolution models to high-resolution structures, *J. Bioenerg. Biomembr. 35*, 337−345.
47. Lepier, A., Graf, R., Azuma, M., Merzendorfer, H., Harvey, W. R., and Wieczorek, H. (1996) The peripheral complex of the tobacco hornworm V-ATPase contains a novel 13-kDa subunit G, *J. Biol. Chem. 271*, 8502−8508.
48. Bernal, R. A., and Stock, D. (2004) Three-Dimensional Structure of the Intact *Thermus thermophilus* H^+-ATPase/Synthase by electron microscopy, *Structure 12*, 1789−1798.

BI051762F